Biogeosciences Discuss., 8, 121–156, 2011
www.biogeosciences-discuss.net/8/121/2011/
doi:10.5194/bgd-8-121-2011

Biogeosciences Discussions

A coupled physical-biological model of the Northern Gulf of Mexico shelf: model description, validation and analysis of phytoplankton variability

K. Fennel[1], R. Hetland[2], Y. Feng[2], and S. DiMarco[2]

[1]Department of Oceanography, Dalhousie University, Halifax, Nova Scotia, Canada
[2]Department of Oceanography, Texas A&M University, College Station, Texas, USA

Received: 16 December 2010 – Accepted: 17 December 2010 – Published: 7 January 2011

Correspondence to: K. Fennel (katja.fennel@dal.ca)

Published by Copernicus Publications on behalf of the European Geosciences Union.

Abstract

The Texas-Louisiana shelf in the Northern Gulf of Mexico receives large inputs of nutrients and freshwater from the Mississippi/Atchafalaya River system. The nutrients stimulate high rates of primary production in the river plume, which contributes to the development of a large and recurring hypoxic area in summer. The mechanistic links between hypoxia and river discharge of freshwater and nutrients are complex as the accumulation and vertical export of organic matter, the establishment and maintenance of vertical stratification, and the microbial degradation of organic matter are controlled by a non-linear interplay of factors. We present results from a realistic, 3-dimensional, physical-biological model that includes the processes thought to be of first order importance to hypoxia formation and demonstrate that the model realistically reproduces many features of observed nitrate and phytoplankton dynamics including observed property distributions and rates. We then contrast the environmental factors and phytoplankton source and sink terms characteristic of three model subregions that represent an ecological gradient from eutrophic to oligotrophic conditions. We analyze specifically the reasons behind the counterintuitive observation that primary production in the light-limited plume region near the Mississippi River delta is positively correlated with river nutrient input. We find that, while primary production and phytoplankton biomass are positively correlated with nutrient load, phytoplankton growth rate is not. This suggests that accumulation of biomass in this region is not primarily controlled bottom up by nutrient-stimulation, but top down by systematic differences in the loss processes. We hypothesize that increased retention of river water in high discharge years explains this phenomenon.

1 Introduction

The Texas-Louisiana shelf in the Northern Gulf of Mexico is dominated by large seasonal inputs of freshwater and inorganic and organic nutrients from the

BGD
8, 121–156, 2011

Mississippi/Atchafalaya River system. The Mississippi River is one of the world's major rivers; it has the third largest drainage basin, is the fifth largest in terms of freshwater discharge and seventh largest in terms of sediment discharge compared with other world rivers (Milliman and Meade, 1983). The Mississippi River drains 41% of the contiguous USA, including agricultural land in Southern Minnesota, Iowa, Illinois and Ohio, which contributes about one third of the nitrogen loading of the river (Goolsby et al., 2000). The greatest nitrogen loading comes from tile-drained fields in the cornbelt of the midwest (David et al., 2010). The mean annual nitrogen load to the Gulf of Mexico of 1.5 Mt yr^{-1} consists of approximately 61% nitrate, 37% organic nitrogen and 2% ammonium (1980–1996 mean), and the nitrate load has approximately tripled from 1970 to the late 90ies (Goolsby et al., 2000).

The large nutrient and freshwater discharge from the Mississippi River contributes to the development of a large recurring hypoxic area on the Texas-Louisiana shelf in summer (Rabalais et al., 2002) and is thought to be detrimental to metazoans such as shrimp and demersal fish (Levin et al., 2009; Ekau et al., 2009). The classic concept often used to explain the development of this hypoxic area is as follows. Inorganic nutrients from the Mississippi fuel high rates of primary production as the discharged river water spreads in buoyant plumes over the shelf, and, as this organic matter sinks below the pycnocline and is respired microbially, oxygen consumption exceeds supply in bottom waters and hypoxia develops. The existence of statistically significant relationships between the annual Mississippi River nitrogen load and the spatial extent of the hypoxic area in summer (Turner et al., 2005; Greene et al., 2009) is consistent with this view. Also, a significant statistical relationship between nitrogen load and primary production was reported for the plume region near the Mississippi delta (Lohrenz et al., 1997) and is often interpreted in support of the classical concept.

On the other hand, a number of findings and ideas have been articulated recently that suggest the classic concept is too simplistic and that other factors are important as well (Rowe and Chapman, 2002; Hetland and DiMarco, 2008; Sylvan et al., 2006; Bianchi et al., 2010; Lehrter et al., 2009). For example, terrestrial organic matter load

BGD
8, 121–156, 2011

probably contributes significantly to oxygen consumption (Bianchi et al., 2010, 2009), stratification is important for hypoxia formation in preventing supply of oxygen below the pycnocline (Wiseman et al., 1997), sediment oxygen demand is not directly related to river nutrient load (Morse and Rowe, 1999; Rowe and Chapman, 2002), spatially varying rates of macrozooplankton grazing affect the rate of phytoplankton accumulation and the amount of organic matter reaching the bottom (Dagg, 1995), and phosphate has been shown to limit primary production during spring (Sylvan et al., 2006). DiMarco et al. (2010) found that bathymetric variations contribute to spatial heterogeneity in near bottom oxygen concentrations. Walker and Rabalais (2006) found no significant relationship between satellite-derived surface chlorophyll and hypoxia development. Lehrter et al. (2009), while confirming the existence of a statistically significant relationship between nutrient load and primary production in the plume near the Mississippi River delta, found no significant relationship between nutrient load and shelf-wide total chlorophyll and no relationship between nutrient load and shelf-wide primary production.

Clearly, the mechanistic link between inorganic river nitrogen loads and hypoxia is not direct as the accumulation of phytoplankton biomass, the sinking of organic matter, the establishment and maintenance of vertical stratification, and the microbial degradation of organic matter are controlled by an interplay of factors and can interact in non-linear ways. Numerical models are invaluable tools for assessing the combined effects of these processes and for untangling their relative importance (see recent review of modeling approaches to hypoxia by Peña et al., 2010). For example, Green et al. (2008) and Eldridge and Roelke (2010) developed ecosystem models for the Mississippi River plume to investigate the response of organic matter production and sedimentation to variable loadings of nitrate and freshwater. Their models are embedded in idealized physical frameworks.

Here we present results from a coupled physical-biological model that includes a realistic 3-dimensional circulation model (Hetland and DiMarco, 2008) and a relatively simple nitrogen cycle model (Fennel et al., 2006). The model includes all processes

BGD
8, 121–156, 2011

that are considered to be of first order importance for hypoxia formation, namely river sources of organic and inorganic nitrogen, which enter the model through the Mississippi River delta and Atchafalaya Bay, light- and nutrient-dependent phytoplankton production, zooplankton grazing, sinking of organic matter, microbial respiration, and a realistic and dynamic representation of horizontal and vertical advection and mixing processes. We present an 8-year simulation comparing simulated distributions of nitrate and chlorophyll and model-predicted rates with available observations. After demonstrating that the model realistically reproduces many observed features of nitrate and phytoplankton dynamics we analyze the environmental differences and phytoplankton source and sink terms along an ecological gradient from a high-nutrient plume region near the Mississippi River delta to a low-nutrient region far from the direct influence of river water. We find that while phytoplankton growth rates are very similar across the gradient, differences in phytoplankton loss terms lead to the markedly different rates of phytoplankton accumulation and different standing stocks along the gradient. We also investigate the question why primary production rates in the plume region are correlated with nitrogen concentrations and river nitrate loads, even though primary production is light-limited in this region and, hence, should not be sensitive to variations in nutrient concentrations and nutrient load.

2 Model description

2.1 Physical model

We use a configuration of the Regional Ocean Modeling System (Haidvogel et al., 2008, ROMS, http://myroms.org) for the Mississippi/Atchafalaya outflow region (Fig. 1). The model grid has 20 vertical, terrain-following layers with increased resolution near the surface and bottom. The horizontal resolution is highest near the Mississippi Delta with up to 1 km and lowest in the southwestern corner with ~20 km; the time step is about 1 min. The main features of the physical set-up are as follows. We use

BGD
8, 121–156, 2011

fourth-order horizontal advection of tracers, third-order upwind advection of momentum, and the Mellor and Yamada (1982) turbulence closure scheme for vertical mixing. The model is initialized on 1 January 1990 using an average profile of temperature and salinity, based on historical hydrographic data, which we assumed to be horizontally uniform. At the boundaries, we imposed radiation conditions (Flather, 1976) for the 3-dimensional velocities with no mean barotropic flow. Temperature and salinity at the boundary are relaxed to a horizontally uniform monthly climatology with a timescale of 10 days for outgoing information and 1 day for incoming information.

Our model is forced with spatially uniform but temporally varying 3-hourly winds from the BURL 1 C-MAN weather station at 28° 54′ N, 89° 25′ W near the major pass of the Mississippi delta. Given the spatial scales of the local wind field (Wang et al., 1998), spatially uniform wind forcing is appropriate for out model domain. We specified surface heat and freshwater fluxes using the climatological fields of da Silva et al. (1994a,b), and freshwater inputs from the Mississippi and Atchafalaya Rivers using daily measurements of transport by the US Army Corps of Engineers at Tabert Landing and Simmesport, respectively. We did not include tides, as they are known to be small in this region (DiMarco and Reid, 1998).

The physical model realistically captures the two distinct modes of circulation over the Texas-Louisiana shelf – the mean offshore flow during upwelling favorable winds in summer and the mean westward (downcoast) flow during downwelling favorable winds for the rest of the year – as described in Hetland and DiMarco (2008). The model also has skill in predicting observed salinity distributions (Hetland, 2010).

2.2 Biological model

The biological component of our model uses the nitrogen cycle model described in Fennel et al. (2006, 2008). The nitrogen cycle model is a relatively simple representation that includes two species of dissolved inorganic nitrogen (nitrate, NO_3, and ammonium, NH_4), one functional phytoplankton group, Phy, chlorophyll as a separate state variable, Chl, to allow for photoacclimation, one functional zooplankton group, Zoo, and

BGD
8, 121–156, 2011

two pools of detritus representing large, fast-sinking particles, LDet, and suspended, small particles, SDet. The representation of nitrogen cycling in the water column is similar to other coupled models (e.g., Oschlies, 2002; Gruber et al., 2006), however, the model's treatment of sediment remineralization, which is critical for model application to continental shelf regions, is unusual.

The model uses an empirical parameterization of sediment denitrification. Specifically, organic matter that reaches the sediment is remineralized in fixed proportions through aerobic and anaerobic remineralization. The fractions are determined using the linear relationship between sediment denitrification and oxygen consumption that Seitzinger and Giblin (1996, their Fig. 1) calculated for a compilation of published measurements (note that their relationship includes production of N_2 gas through anammox; the term denitrification is used here to denote canonical denitrification following Devol (2008) and includes all processes that produce N_2 gas). This empirical relationship was based on 50 data points. Fennel et al. (2009) compiled a larger data set including 648 data points across a range of aquatic environments, including from the coastal Gulf of Mexico, and reevaluated the linear regression. This new relationship deviates little from the previously published one, although the coefficient of determination for the larger data set is smaller than that of Seitzinger and Giblin (1996). The details of the nitrogen formulation are given in Fennel et al. (2006) and are not repeated here for the sake of brevity.

In combination with the freshwater discharge described above, the model receives inorganic and organic nutrients. Specifically nitrate, ammonium and particulate nitrogen fluxes (the latter is assumed to enter the pool of small detritus in the model) are specified (Fig. 2) based on monthly nutrient flux estimates from the US Geological Survey (Aulenbach et al., 2007). Particulate organic nitrogen fluxes are determined as the difference between total Kjeldahl nitrogen and ammonium. To account for light attenuation in the river plume we introduced a salinity-dependent attenuation term in the calculation of the photosynthetically active radiation I at depth z as follows

$$I(z) = I_0 \cdot \mathrm{par} \cdot e^{-zK - zK_{\mathrm{salt}} - K_{\mathrm{chl}} \int_0^z \mathrm{Chl}(\zeta) d\zeta}, \quad (1)$$

BGD
8, 121–156, 2011

where I_0 is the incoming light just below the sea surface, par is the fraction of light that is available for photosynthesis, K and K_{chl} are the light attenuation coefficients for water and chlorophyll, respectively. The salinity-dependent attenuation is $K_{salt}=\max(-0.024+0.89S,0)$ where S is salinity.

Here, we present an 8-year simulation starting on 1 January 1990. The biological variables NH_4, Phy, Chl, Zoo, SDet and LDet were initialized with small constant values. NO_3 and O_x were initialized with horizontally homogenous mean winter profiles based on available in situ data. At the open boundaries NO_3 and O_x were prescribed using horizontally homogenous profiles based on measurements from the LATEX and NEGOM cruises (Nowlin Jr. et al., 1998; Jochens et al., 2002). All other biological state variables at the boundary are set to small positive values.

3 Results

Here we describe major features of the simulated biological variables, focusing primarily on nutrients and phytoplankton, and compare simulated variables and rates to available observations. We first compare simulated surface nitrate and chlorophyll distributions and primary production rates to observations, then describe the climatological seasonal cycle of simulated nitrate, phytoplankton and zooplankton for three sub-regions of the model domain, which represent an ecological gradient, and then compare simulated phytoplankton growth, zooplankton grazing and organic matter sedimentation rates to observational estimates.

3.1 Surface nitrate concentrations

A comparison of simulated surface nitrate concentrations with the observations of Sylvan et al. (2006) is shown in Fig. 3. Since Sylvan et al.'s observations are from the years 2000 to 2004 we cannot compare these measurements directly to the simulation. However, the observations illustrate well the spatial patterns of surface nitrate,

BGD
8, 121–156, 2011

their temporal evolution and interannual differences and thus represent a useful comparison. We chose to show the simulated nutrients from 1993 and 1994 as these years represent a strong contrast in terms of river nitrate load (see Fig. 2; 1993 had the highest discharge and nitrogen load during the simulation period).

During spring and summer, the observed surface nitrate distribution on the shelf is determined to first order by the dilution/mixing of high-nitrate fresh water and by the uptake of nitrate by phytoplankton, consistent with the observations described in Lohrenz et al. (1999). During May of 2001 and 2004, the surface nitrate observations most closely resemble a conservative mixing relationship (Fig. 3, top panels). The difference in freshwater nitrate concentration, which was about twice as high in May 2001 (~230 mmol N m^{-3}) compared to May 2004 (~94 000 mmol N m^{-3}), propagates to intermediate salinities of 20 to 30 where again nitrate concentrations in 2001 are about double those of 2004. Low nitrate concentrations of <3 mmol N m^{-3} are restricted to high salinities (>32) in May. Over the course of the summer, surface nitrate is drawn down at intermediate salinities. For example, in 2004 the majority of samples taken at intermediate salinities of 20–30 have low nitrate concentrations of <3 mmol N m^{-3} in July, and by September of 2001 all samples at intermediate salinities have low nitrate concentrations (Fig. 3). The observations also illustrate interannual variability in both, nitrogen load and freshwater input, with lower nitrate concentrations at intermediate salinities in 2002 and 2004 compared to 2001, and generally fresher shelf waters in 2004 compared to 2002.

The simulated concentrations show patterns similar to the observations in terms of the monthly evolution and interannual differences. As seen in the observations, the simulated surface nitrate concentrations resemble a conservative mixing relationship most closely in May. The different river end member concentrations from the Mississippi and Atchafalaya Rivers are clearly distinguishable (Fig. 3, top panels). Over the course of the summer, nitrate is drawn down at intermediate salinities, but there are marked differences between 1993 and 1994. In 1993, supply of nitrate from the rivers is elevated throughout the summer leading to relatively high nitrate concentrations (20–

BGD
8, 121–156, 2011

80 mmol N m^{-3}) at low salinities (10–15) and elevated nitrate (0–20 mmol N m^{-3}) at intermediate salinities (10–20) in September. Surface nitrate is consistently lower in August and September of 1994, which is a more typical year.

3.2 Surface chlorophyll and primary production

We now compare the simulated surface chlorophyll to observations derived from the SeaWiFS satellite. The SeaWiFS data set we used includes observations from September 1998 to December 2004 and does not overlap with the simulation period. Hence, we cannot compare interannual variations and use a monthly climatology instead. Chlorophyll concentrations are observed to be highest in the freshwater plumes (>30 mg m^{-3}) and show a generally decreasing tendency from high concentrations near shore (1 to 10 mg m^{-3}) to values <1 mg m^{-3} near the shelf break (Fig. 4). Chlorophyll concentrations are lowest in winter, increase in spring, remain high throughout summer, and decrease in early fall (Fig. 4). The model captures these spatial and temporal patterns in average chlorophyll well. Spatial patterns are compared in Fig. 4 for April to September and statistical measures of model-data agreement are given in Table 1.

The climatological annual cycles of surface chlorophyll averaged for the delta, intermediate and far-field regions (see Fig. 1) are shown in Fig. 5. The climatological annual cycle is described well by the model in the delta region, although the accumulation of phytoplankton in spring is delayed by a month in the model. Maximum chlorophyll concentrations in summer are higher than in the SeaWiFS climatology in several years, in particular during the first four years of the simulation, which is not surprising as nitrogen loads were markedly higher from 1990 to 1995 compared to the SeaWiFS data period from 1999 to 2004 (the annual Mississippi River nitrate loads were 88×10^4, 74×10^4 and 58×10^4 metric tons, respectively, for 1990–1994, 1995–1998 and 1999–2004). The largest summer chlorophyll concentrations are predicted for 1993 (the year with highest discharge and nitrogen load). For the intermediate region, the range and

BGD
8, 121–156, 2011

temporal evolution of chlorophyll also agrees well with the climatology, in particular for the years 1992 and 1996 to 1998. In 1993 the model predicts higher than average chlorophyll concentrations as one would expect given the disproportionate nitrogen load that year. Also, the occasionally elevated chlorophyll values in summer are likely due to the larger nitrogen loads, especially for the first half of the simulation period. For the far-field region the model-simulated values agree well with the climatology from 1994 through 1998, i.e. the years when Mississippi River nitrogen loads were closer to loads observed during our SeaWiFS data period, while concentrations are above the climatology from 1990 to 1994.

We also compared simulated rates of primary production, averaged for the delta and intermediate regions, to the observations of Lohrenz et al. (1997) (Fig. 6). Observed rates range from typically $\sim$1 g C m^{-2} d^{-1} in fall or winter to maximum values between 3 and 4 g C m^{-2} d^{-1} during spring and summer, but are highly variable, as indicated by the large standard deviations associated with some values and the large differences in observations made only a few days apart (e.g. in spring of 1993). The simulated rates agree well with the observations in terms of magnitude and temporal patterns, especially in 1990 and 1992.

3.3 Seasonal cycle of nitrate, phytoplankton and zooplankton

In our simulation, the delta, intermediate and far-field regions differ markedly in terms of nutrient supply and evolution of phytoplankton and zooplankton, as can be seen in the climatological cycles of their mixed layer averaged nitrate concentrations and phytoplankton and zooplankton biomasses (Fig. 7). In the delta region, average nitrate is near or above 10 mmol N m^{-3} all year (i.e. well above concentrations near or below 1 mmol N m^{-3} considered limiting to phytoplankton). A reduction in nitrate occurs from April to October (by $\sim$25 mmol N m^{-3}) through dilution (i.e. export of nitrate across the delta region's boundary) and phytoplankton uptake, and nitrate is replenished again during the other months of the year through river input and, to a lesser degree, remineralization. Average nitrate concentrations in the intermediate region are

BGD
8, 121–156, 2011

near 10 mmol N m^{-3} during winter and early spring but drop to limiting concentrations between April and July, and remain low for the following 4 to 5 months. In the far-field region, average mixed layer nitrate is always at limiting concentrations.

Average mixed layer phytoplankton biomasses in the delta and intermediate regions are near 2 mmol N m^{-3} from December to March and begin to increase and diverge in April, reaching maximum concentrations of 8 mmol N m^{-3} in the delta region in July and 4 mmol N m^{-3} in the intermediate region (Fig. 7). In contrast, maximum zooplankton concentrations are very similar (~4 mmol N m^{-3} in June) in the delta and intermediate regions and remain similar throughout the whole seasonal cycle. In the far-field region, average mixed layer phytoplankton biomass is almost stationary near 1 mmol N m^{-3}, while zooplankton biomass exhibits a seasonal cycle with increasing concentrations in spring. During spring and early summer, average mixed layer zooplankton biomass exceeds that of phytoplankton in the far-field region.

3.4 Phytoplankton growth rates

We calculated the mixed layer averages of the phytoplankton community growth rate $\mu=\mu_{max}f(I)(L_{NO_3}+L_{NH_4})$ and plotted the climatological monthly means for the 8-year simulation period in Fig. 8a. Interestingly the simulated growth rates are very similar in all three regions with minima between 0.2 and 0.4 d^{-1} in fall and maxima between 1 and 1.4 d^{-1} in summer (Fig. 8d). The simulated rates can be compared with the observed rates of Fahnenstiel et al. (1995), who reported taxon-specific growth rates of the dominant phytoplankton taxa for the delta and intermediate regions for March 1991 and July/August 1990. These observed growth rates varied considerably between taxa with lowest values of <0.1 d^{-1} and maximum rates of 3 d^{-1}. The observed mean and median growth rates of Fahnenstiel et al. (1995) were 0.5 and 0.4 d^{-1}, respectively, for March 1991 and agree remarkably well with the model simulated growth rates of 0.5 d^{-1} for the delta region and 0.7 d^{-1} for the intermediate region for March 1991 (not shown). The observed mean and median growth rates for July/August 1990 were 1.3

BGD
8, 121–156, 2011

and 1.0 d^{-1}, which also agree very well with the simulated rates of 1.1 d^{-1} for July 1990 and 0.8 d^{-1} for August 1990 in the delta region (not shown).

3.5 Zooplankton grazing and other loss terms

The zooplankton variable in our model is assumed to primarily represent macrozooplankton such as copepods, which have lower growth rates than phytoplankton during bloom conditions and thus lag behind phytoplankton in spring. Microzooplankton on the other hand grow at similar rates as small phytoplankton and are thus able to respond to increasing phytoplankton concentrations without delay. These microzooplankton grazers are not represented explicitly in our model, however, the first order mortality loss of phytoplankton can be interpreted to represent the grazing loss of microzooplankton. This first order mortality loss is largest in May, June and July in the delta region with mean values of 70–100 mg C m^{-2} d^{-1}, and smaller in the intermediate region with rates about half of those in the delta region (Fig. 9e). The first order mortality loss is much smaller in the far-field region with summer rates of about 15 mg C m^{-2} d^{-1}. The macrozooplankton grazing losses are higher than the first order mortality losses with mean values of about 150 mg C m^{-2} d^{-1} in May and June in the delta and intermediate regions, and between 40–50 mg C m^{-2} d^{-1} in the far-field region (Fig. 9a). These rates can be compared with the copepod grazing rates determined by Dagg (1995), who estimated daily ingestion rates of 537 and 92 mg C m^{-2} d^{-1} at stations in the delta and intermediate regions, respectively, in September of 1991, and 166 and 147 mg C m^{-2} d^{-1} at the same stations in May of 1992. Both May 1992 rates and the September 1991 intermediate region rate are similar to the model-simulated mean rates, however, the rate observed in the delta region in September 1991 is much higher than the model-simulated mean rate for the region, which may in part be due to averaging. The simulated daily rates reached values up to 320 mg C m^{-2} d^{-1}, which are closer to the observed rate of 537 mg C m^{-2} d^{-1}. Simulated grazing rates in the far-field region are smaller with summer maxima between 40 and 80 mg C m^{-2} d^{-1}.

BGD
8, 121–156, 2011

The simulated monthly mean aggregation rates, which are indicative of the sedimentation flux, range between 0.1 and 0.45 d^{-1} in the delta region and between 0.05 and 0.25 d^{-1} in the intermediate region (note that aggregation losses in Fig. 9c are given in a different unit). Fahnenstiel et al. (1995) estimated taxon-specific sedimentation rates between <0.001 and 1.0 d^{-1} in the delta and intermediate region and found the largest sedimentation fluxes associated with diatoms. While these rates are not representative of the phytoplankton community and thus cannot be compared directly to the model-simulated rates it is worthwhile noting that the model-simulated rates are within the observed range. Aggregation loss has the most pronounced spatial dependence of all three biological loss terms. In the delta region, aggregation loss is similar in magnitude to the grazing and mortality combined. In the intermediate region, aggregation loss is similar to the first order mortality losses, but much smaller than the grazing term. In the far region, aggregation loss makes up less than half of the first order mortality term and is much smaller then the grazing term.

4 Discussion

Our model simulation agrees well with observed spatial and temporal patterns and distributions of surface nitrate, surface chlorophyll and primary production. Simulated rates of primary production, phytoplankton growth, and zooplankton grazing also agree well with the corresponding observed rates. Thus, we feel that the simulations capture phytoplankton dynamics on the Texas-Louisiana shelf well enough to investigate the underlying drivers in the model and make inferences about processes in the natural system. First, we discuss which factors limit phytoplankton growth in the delta, intermediate and far-field regions and contrast the relative importance of different phytoplankton losses in these regions. We then examine relationships between monthly mean primary production in the delta region and Mississippi River nitrate load in order to elucidate why primary production in this region is correlated with nitrate load even though phytoplankton growth is not limited by nitrate.

BGD
8, 121–156, 2011

4.1 Factors controlling plankton growth and accumulation of biomass

We first investigate the factors limiting phytoplankton growth in the three regions. We calculated the mixed layer mean light-limitation term $f(I)$ and show its climatological monthly means for the 8-year simulation period in Fig. 8b. Small values of $f(I)$ indicate light-limitation, while values near 1 correspond to no light-limitation. We also calculated the mixed layer mean values of the nutrient-limitation term $L_{TOT}=L_{NO_3}+L_{NH_4}$ and show its climatological monthly means in Fig. 8c. Again, values of L_{TOT} near 1 correspond to no nutrient-limitation, while small values indicate nutrient-limitation.

As expected, light-limitation is strongest in the delta and weakest in the far-field region. There is a pronounced seasonal cycle to the light-limitation term that is coherent in all three regions with strongest light-limitation in late fall and winter and lowest light-limitation in early summer. Except for fall, where light-limitation in the intermediate and far-field regions is of similar magnitude, there is always a pronounced spatial gradient with strongest light-limitation in the delta region and weaker light-limitation in the intermediate and far-field regions. The patterns of nutrient limitation are opposite in many respects. There is essentially no nutrient-limitation in the delta region; nutrient-limitation increases toward the intermediate and far-field regions. In all three regions nutrient-limitation is more pronounced in the fall and weakest in the spring.

The ratio of $f(I)$ and L_{TOT} (Fig. 8d) can be interpreted as a measure of the relative importance of light- versus nutrient-limitation (small values correspond to light-limitation) and illustrates that the delta region is strongly light-limited all year, while the far-field region is strongly nutrient-limited in summer, and the intermediate region is midway between the two. Seasonal changes in this ratio are small in the delta region, and most pronounced in the far-field region where limitation by light becomes more important in winter. Given the pronounced differences in limiting factors and in nutrient, chlorophyll and phytoplankton concentrations between the delta, intermediate and far-field regions (e.g., Figs. 5 and 7), it is maybe surprising that their community growth rates are very similar (Fig. 8a). However, the phytoplankton growth rate is determined by the product

BGD
8, 121–156, 2011

of $f(I)$ and L_{TOT}, which largely compensate for each other across the spatial gradient, and is modulated only by the temperature-dependent value of the maximum growth rate, which is very similar in all three regions, but has a pronounced seasonal cycle.

Despite similar growth rates in all three regions, phytoplankton concentrations and primary production are much higher (by a factor of 2 to 8) in the delta and intermediate regions than in the far-field region from May through August. Also, phytoplankton concentrations and primary production are much higher in the delta region compared to the intermediate region in summer. These differences can only be explained by spatially differing phytoplankton loss terms.

In the geographic regions considered here, phytoplankton can be lost by physical transport across the region boundaries and by biological losses (i.e. grazing-induced mortality, sinking). The sum of the climatological biological loss terms (described individually in Sect. 3.5 above) varies between a minimum of $\sim$50 mg C m^{-2} d^{-1} in winter in all three regions, but markedly different maximum values in early summer of 500, 250 and 50 mg C m^{-2} d^{-1} in the delta, intermediate and far-field regions, respectively (Fig. 9d). When comparing climatological primary production and the sum of biological losses (Fig. 9b and d) it is obvious that they follow a very similar pattern and have similar magnitudes. Accumulation of phytoplankton is determined by the imbalance of production and losses, which is shown in Fig. 9f for primary production and biological losses.

In the delta region, there is a positive imbalance from April to July reaching a maximum of about 60 mg C m^{-2} d^{-1} in June. In May and June this imbalance corresponds to about 10% of primary production, in other words, 10% of primary production can accumulate while about $\sim$90% is lost to grazing, mortality and sinking. During the rest of the year the phytoplankton standing stock is in balance or declining (the imbalance between primary production and biological losses is near zero or negative).

In the intermediate region, the imbalance of primary production and biological losses is negative most of the year, approaching zero only in winter, despite the accumulation of phytoplankton in spring when it is doubling its standing stock compared to winter

BGD
8, 121–156, 2011

values (Fig. 7). We infer that advection and mixing of phytoplankton results in a net transport from the delta to the intermediate region supporting the accumulation of phytoplankton biomass in the latter. A similar picture emerges for the far-field region, where primary production and biological losses are in balance for most of the year, except during spring and early summer when biological losses exceed primary production, while the phytoplankton standing stock is increasing slightly. This indicates that physical transport of phytoplankton into the far-field region occurs at this time.

In summary, small mismatches between primary production and phytoplankton losses can explain the pronounced regional differences in phytoplankton standing stock and primary production that are observed to occur between the delta, intermediate and far-field region.

4.2 Correlations between primary production and nutrients for the delta region

In our model, phytoplankton growth in the delta region is not limited by nitrate (see Figs. 7 and 8), which is in agreement with observations by Lohrenz et al. (1999) that indicate phytoplankton is light-limited in this region. Yet, a correlation between Mississippi nitrogen load and primary production has been shown to exist for this region by Lohrenz et al. (1997) and, more recently based on a larger data set, by Lehrter et al. (2009). The existence of this correlation is often interpreted as a bottom up effect of river nutrients directly stimulating primary production. However, this interpretation is in contradiction with the observed lack of nutrient limitation. Our model simulation allows us to examine the nature of this relationship in more detail.

First, we examine the relationship between monthly mean primary production in the delta region and monthly NO_3 load from the Mississippi over the 8-year simulation period. Two distinct linear relationships with very different slopes exist (Fig. 10a). From October through March there is a statistically significant linear relationship between monthly primary production and monthly NO_3 load with a slightly negative slope. In other words, during this period primary production is essentially insensitive to NO_3 load. From May through September a different and statistically significant relationship

BGD
8, 121–156, 2011

emerges with a positive slope. During this period, primary production is elevated when NO_3 load and, by implication, surface DIN concentrations are high (Fig. 10a, the same pattern emerges when primary production is related to monthly mean DIN concentrations in the delta region instead of NO_3 load; see Table 2). In other words, the system shifts from a phase of insensitivity to NO_3 load (or DIN concentration) in winter and early spring to a phase when primary production appears to be sensitive to NO_3 load in late spring and summer. The shift occurs in March-April when phytoplankton growth rates are already near their maximum values.

This bi-modal pattern supports the previously reported relationships, which focused on spring and summer, i.e. one of the two distinct periods we identified. Lohrenz et al. (1997) used data primarily from late spring and summer in their analysis; no data points for winter and only one early fall data point were included and their only measurement from early spring (March 1991) was excluded (otherwise the resulting relationship was not significant). Lehrter et al. (2009) repeated the analysis after adding 7 more data points (all spring and summer observations) and again found a significant relationship, although with a much smaller R^2=0.20 instead of R^2=0.58 in Lohrenz et al. (1997).

The question now is: How can primary production, which is not limited by nutrients in this region, be correlated with nutrient load and concentration? One possibility is that the correlation simply results from the fact that both, primary production and NO_3 load (or DIN concentration) have seasonal cycles. In fact, similar significant correlations result when the average seasonal cycle of primary production and NO_3 load (or DIN concentration) is used (Table 2). We thus removed the annual cycle from the time series of monthly primary production and NO_3 load (and DIN concentration) and investigated the resulting anomalies for positive correlations (Fig. 10b). A highly significant positive correlation ($p<10^{-7}$) between primary production anomalies and NO_3 load anomalies for the period from June through September emerges. In other words, interannual differences in NO_3 load are reflected in variations in primary production in summer (not in spring). However, when investigating the monthly mean growth rate anomalies of the

BGD
8, 121–156, 2011

phytoplankton community, no significant relationship with NO_3 load anomalies (and DIN concentration anomalies) exists (Fig. 10c). The lack of a relationship between nutrient load (or concentration) and community growth rates is consistent with our expectation that a phytoplankton community that is not limited by nutrients also should not be sensitive to perturbations in nutrient concentrations. Considering that primary production is the product of instantaneous phytoplankton community growth rate and accumulated phytoplankton biomass, the relationship between primary production and NO_3 load could simply reflect a relationship between accumulated phytoplankton biomass and NO_3 load (or concentration). In fact, there is a highly significant relationship ($p<10^{-11}$) between monthly phytoplankton biomass anomalies and NO_3 load for June through September (Fig. 10d). Thus, the positive correlation between primary production and NO_3 load in the light-limited region of the plume is not primarily a bottom-up effect, but results from differences in phytoplankton accumulation likely due to differences in loss terms (i.e., advection and mixing, grazing and sedimentation).

We believe that advection is the primary process responsible for interannual differences in phytoplankton accumulation with increased retention of phytoplankton during years with higher discharge. Interannual variations in river NO_3 concentration are much smaller than interannual variations in streamflow; NO_3 load is the product of these two variables. Changes in streamflow likely cause altered circulation patterns over the shelf. Increased accumulation during anomalously high streamflow years (corresponding to high NO_3 load because NO_3 load and streamflow are correlated) suggests that a retaining circulation pattern is formed during wetter years. One possible mechanism is the enhancement of a recirculating gyre east of the Mississippi River delta (Ichiye, 1960; Wiseman Jr et al., 1982; Hetland and DiMarco, 2008). Fong and Geyer (2002) demonstrated the counter-intuitive result that increased river flow will decrease downstream coastal current transport, thereby increasing retention in the recirculating bulge that forms offshore of a freshwater source. Investigation into the potential causes of hydrodynamic retention of plankton under high discharge conditions is beyond the scope of this paper, and will be the focus of future studies.

BGD
8, 121–156, 2011

5 Conclusions

We presented an 8-year simulation of a realistic physical-biological model for the Texas-Louisiana Shelf. Our model describes the spatial and temporal patterns of nitrate and phytoplankton in agreement with observations and predicts rates of primary production and grazing that agree with experimentally determined rates. In the model differences in phytoplankton biomass and primary production across the ecological gradient from the delta, to the intermediate and far-field region are not primarily driven by differences in phytoplankton growth rates, but by differences in phytoplankton losses. While phytoplankton growth rates are similar, there are pronounced spatial differences in the rate of phytoplankton accumulation and phytoplankton losses, and there is a net transport of phytoplankton from the delta to the intermediate region and into the far-field region.

Our model shows that the existence of a statistically significant correlation between primary production and nitrogen load in the delta region near the Mississippi River delta does not reflect a direct stimulation of phytoplankton growth by nutrients as expected given the lack of nutrient-limitation in this region. When investigating this relationship it is necessary to first remove the seasonal cycle or, since this is less practical with sparse observational data sets, take into account the autocorrelation between primary production and nitrogen load by increasing the degrees of freedom and adjusting the *p*-levels appropriately. We find a statistically significant relationship between anomalies of primary production and nitrogen load for the months of June through September. We also find a statistically significant relationship between the anomalies of phytoplankton biomass and nitrogen load for the same months, but not for the anomalies of phytoplankton growth rates and nitrogen load. Since primary production is the product of growth rate and phytoplankton biomass the relationship between primary production and nitrogen load simply reflects the relationship between phytoplankton biomass and nitrogen load, which results from differences in phytoplankton accumulation likely due to differences in loss terms. We hypothesize that higher rates of biomass accumulation in high discharge years result from stronger retention of river water near the delta.

BGD
8, 121–156, 2011

Acknowledgements. We thank Jason Sylvan and James Ammerman for making their nutrient data available to us. This work was supported by NOAA CSCOR grants NA06N0S4780198 and NA09N0S4780208 and Cooperative Agreement M07AC12922 with the US Department of the Interior (Minerals Management Service). NOAA NGOMEX publication no. 141.

References

Aulenbach, B., Buxton, H., Battaglin, W., and Coupe, R.: Streamflow and nutrient fluxes of the Mississippi-Atchafalaya River Basin and subbasins for the period of record through 2005, Open-file report 2007-1080, US Geological Survey, , 2007. 127

Bianchi, T., DiMarco, S., Smith, R., and Schreiner, K.: A gradient of dissolved organic carbon and lignin from Terrebonne-Timbalier Bay estuary to the Louisiana shelf (USA), Mar. Chem., 117, 32–41, 2009. 124

Bianchi, T., DiMarco, S., Cowan Jr., J., Hetland, R., Chapman, P., Day, J., and Allison, M.: The science of hypoxia in the Northern Gulf of Mexico: a review, Sci. Total Environ., 408, 1471–1484, 2010. 123, 124

Dagg, M.: Copepod grazing and the fate of phytoplankton in the Northern Gulf of Mexico, Cont. Shelf Res., 15, 1303–1317, 1995. 124, 133

David, M., Drinkwater, L., and McIsaac, G.: Sources of nitrate yields in the Mississippi River Basin, J. Environ. Qual., 39, 1657–1667, 2010. 123

Devol, A. H.: Denitrification including anammox, chapt. 6: in: Nitrogen in the Marine Environment, edited by: Capone, D., Carpenter, E., Mullholland, M., and Bronk, D., Elsevier, Burlington, Amsterdam, San Diego, London, 263–302, 2008. 127

DiMarco, S. and Reid, R.: Characterization of the principal tidal current constituents on the Texas-Louisiana shelf, J. Geophys. Res., 103, 3093–3109, 1998. 126

DiMarco, S., Chapman, P., Walker, N., and Hetland, R.: Does local topography control hypoxia on the Eastern Texas-Louisiana shelf?, J. Marine Syst., 80, 25–35, 2010. 124

Ekau, W., Auel, H., Pörtner, H.-O., and Gilbert, D.: Impacts of hypoxia on the structure and processes in pelagic communities (zooplankton, macro-invertebrates and fish), Biogeosciences, 7, 1669–1699, doi:10.5194/bg-7-1669-2010, 2010. 123

Eldridge, P. and Roelke, D.: Origins and scales of hypoxia on the Louisiana shelf: importance of seasonal plankton dynamics and river nutrients and discharge, Ecol. Model., 221, 1028–1042, 2010. 124

Fahnenstiel, G., McCormick, M., Lang, G., Redalje, D., Lohrenz, S., Markowitz, M., Wag-

BGD

8, 121–156, 2011

oner, B., and Carrick, H.: Taxon-specific growth and loss rates for dominant phytoplankton populations from the Northern Gulf of Mexico, Mar. Ecol.-Prog. Ser., 117, 229–239, 1995. 132, 134

Fennel, K., Wilkin, J., Levin, J., Moisan, J., O'Reilly, J., and Haidvogel, D.: Nitrogen cycling in the Middle Atlantic Bight: results from a three-dimensional model and implications for the North Atlantic nitrogen budget, Global Biogeochem. Cy., 20, GB3007, doi:10.1029/2005GB002456, 2006. 124, 126, 127

Fennel, K., Wilkin, J., Previdi, M., and Najjar, R.: Denitrification effects on air-sea CO_2 flux in the coastal ocean: simulations for the Northwest North Atlantic, Geophys. Res. Lett., 35, L24608, doi:10.1029/2008GL036147, 2008. 126

Fennel, K., Brady, D., DiToro, D., Fulweiler, R., Gardner, W., Giblin, A., McCarthy, M., Rao, A., Seitzinger, S., Thouvenot-Korppoo, M., and Tobias, C.: Modeling denitrification in aquatic sediments, Biogeochemistry, 93, 159–178, 2009. 127

Flather, R.: A tidal model of the Northwest European continental shelf, Mem. Soc. R. Sci. Liege, 10, 141–164, 1976. 126

Fong, D. and Geyer, W.: The alongshore transport of freshwater in a surface-trapped river plume, J. Phys. Oceanogr., 32, 957–972, 2002. 139

Goolsby, D., Battaglin, W., Aulenbach, B., and Hooper, R.: Nitrogen flux and sources in the Mississippi River Basin, Sci. Total Environ., 248, 75–86, 2000. 123

Green, R., Breed, G., Dagg, M., and Lohrenz, S.: Modeling the response of primary production and sedimentation to variable nitrate loading in the Mississippi River plume, Cont. Shelf Res., 28, 1451–1465, 2008. 124

Greene, R., Lehrter, J., and Hagy, J.: Multiple regression models for hindcasting and forecasting midsummer hypoxia in the Gulf of Mexico, Ecol. Appl., 19, 1161–1175, 2009. 123

Gruber, N., Frenzel, H., Doney, S., Marchesiello, P., McWilliams, J., Moisan, J., Oram, J., Plattner, G., and Stolzenbach, K.: Eddy-resolving simulation of plankton ecosystem dynamics in the California Current System, Deep-Sea Res. Pt. I, 53, 1483–1516, 2006. 127

Haidvogel, D. B., Arango, H., Budgell, W. P., Cornuelle, B. D., Curchitser, E., Di Lorenzo, E., Fennel, K., Geyer, W. R., Hermann, A. J., Lanerolle, L., Levin, J., McWilliams, J. C., Miller, A. J., Moore, A. M., Powell, T. M., Shchepetkin, A. F., Sherwood, C. R., Signell, R. P., Warner, J. C., and Wilkin, J.: Ocean forecasting in terrain-following coordinates: formulation and skill assessment of the regional ocean modeling system, J. Comput. Phys., 227, 3595–3624, 2008. 125

BGD
8, 121–156, 2011

Hetland, R. and DiMarco, S.: How does the character of oxygen demand control the structure of hypoxia on the Texas-Louisiana continental shelf?, J. Marine Syst., 70, 49–62, 2008. 123, 124, 126, 139
Hetland: 2010. 126
Ichiye, T.: On the hydrography of the Mississippi Delta, Oceanogr. Mag., 11, 65–78, 1960. 139
Jochens, A., DiMarco, S., Nowlin Jr., W. D., Reid, R., and Kennicutt II, M.: Northeastern Gulf of Mexico chemical oceanography and hydrography study, Synthesis report, OCS study MMS 2002, Tech. rep., US Department of the Interior, Minerals Management Service, Gulf of Mexico OCS Region, New Orleans, LA, 2002. 128
Lehrter, J., Murrell, M., and Kurtz, J.: Interactions between freshwater input, light, and phytoplankton dynamics on the Louisiana continental shelf, Cont. Shelf Res., 29, 1861–1872, 2009. 123, 124, 137, 138
Levin, L. A., Ekau, W., Gooday, A. J., Jorissen, F., Middelburg, J. J., Naqvi, S. W. A., Neira, C., Rabalais, N. N., and Zhang, J.: Effects of natural and human-induced hypoxia on coastal benthos, Biogeosciences, 6, 2063–2098, doi:10.5194/bg-6-2063-2009, 2009. 123
Lohrenz, S., Fahnenstiel, G., Redalje, D., Lang, G., Chen, X., and Dagg, M.: Variations in primary production of Northern Gulf of Mexico continental shelf waters linked to nutrient inputs from the Mississippi River, Mar. Ecol.-Prog. Ser., 155, 45–54, 1997. 123, 131, 137, 138
Lohrenz, S., Fahnenstiel, G., Redalje, D., Lang, G., Dagg, M., Whitledge, T., and Dortch, Q.: Nutrients, irradiance, and mixing as factors regulating primary production in coastal waters impacted by the Mississippi River plume, Cont. Shelf Res., 19, 1113–1141, 1999. 129, 137
Mellor, G. and Yamada, T.: Development of a turbulence closure model for geophysical fluid problems, Rev. Geophys., 20, 851–875, 1982. 126
Milliman, J. and Meade, R.: World-wide delivery of river sediment to the oceans, J. Geol., 91, 1–21, 1983. 123
Morse, J. and Rowe, G.: Benthic biogeochemistry beneath the Mississippi River plume, Estuar. Coast., 22, 206–214, 1999. 124
Nowlin Jr., W. D., Jochens, A. E., Reid, R. O., and DiMarco, S. F.: Texas-Louisiana shelf circulation and transport processes study, Synthesis report. Vol. I and II. OCS study MMS 98-0035 and MMS 98-0036, Tech. rep., US Department of the Interior, Minerals Management Service, Gulf of Mexico OCS Regional Office, New Orleans, LA, 1998. 128
Oschlies, A.: Improved representation of upper-ocean dynamics and mixed layer depths in

BGD
8, 121–156, 2011

a model of the North Atlantic on switching from eddy-permitting to eddy-resolving grid resolution, J. Phys. Oceanogr., 32, 2277–2298, 2002. 127
Peña, M. A., Katsev, S., Oguz, T., and Gilbert, D.: Modeling dissolved oxygen dynamics and hypoxia, Biogeosciences, 7, 933–957, doi:10.5194/bg-7-933-2010, 2010. 124
Rabalais, N., Turner, R., and Wiseman Jr., W.: Gulf of Mexico Hypoxia, aka "The Dead Zone", Ann. Rev. Ecol. Syst., 33, 235–263, 2002. 123
Rowe, G. and Chapman, P.: Continental shelf hypoxia: some nagging questions, Gulf Mexico Sci., 20, 153–160, 2002. 123, 124
Seitzinger, S. and Giblin, A.: Estimating denitrification in North Atlantic continental shelf sediments, Biogeochemistry, 35, 235–260, 1996. 127
da Silva, A., Young-Molling, C., and Levitus, S.: Atlas of surface marine data 1994, vol. 3. Anomalies of fluxes of heat and momentum, NOAA Atlas NESDIS 8, Natl. Oceanic and Atmos. Admin., Silver Spring, MD, 1994a. 126
da Silva, A., Young-Molling, C., and Levitus, S.: Atlas of surface marine data 1994, vol. 4, Anomalies of fresh water fluxes, NOAA Atlas NESDIS 9, Natl. Oceanic and Atmos. Admin., Silver Spring, MD, 1994b. 126
Sylvan, J., Dortch, Q., Nelson, D., Brown, A., Morrison, W., and Ammerman, J.: Phosphorus limits phytoplankton growth on the Louisiana shelf during the period of hypoxia formation, Environ. Sci. Technol, 40, 7548–7553, 2006. 123, 124, 128
Turner, R., Rabalais, N., Swenson, E., Kasprzak, M., and Romaire, T.: Summer hypoxia in the Northern Gulf of Mexico and its prediction from 1978 to 1995, Mar. Environ. Res., 59, 65–77, 2005. 123
Walker, N. and Rabalais, N.: Relationships among satellite chlorophyll-*a*, river inputs, and hypoxia on the Louisiana continental shelf, Gulf of Mexico, Estuar. Coast., 29, 1081–1093, 2006. 124
Wang, W., Nowlin Jr., W., and Reid, R.: Analyzed surface meteorological fields over the Northwestern Gulf of Mexico for 1992–94: mean, seasonal, and monthly patterns, Mon. Weather Rev., 126, 2864–2883, 1998. 126
Wiseman Jr., W., Murray, S., Bane, J., and Tubman, M.: Physical environment of the Louisiana Bight, Contrib. Mar. Sci., 25, 109–120, 1982. 139
Wiseman, W., Rabalais, N., Turner, R., Dinnel, S., and MacNaughton, A.: Seasonal and interannual variability within the Louisiana coastal current: stratification and hypoxia, J. Marine Syst., 12, 237–248, 1997. 124

BGD
8, 121–156, 2011

Table 1. Statistics corresponding to the chlorophyll model-data comparisons shown in Fig. 4. RMS=$\sqrt{\frac{1}{n}\sum_{i=1}^{n}(x_i^{\mathrm{obs}}-x_i^{\mathrm{mod}})^2}$ (in units of mg Chl m^{-3}), corr=$\sum_{i=1}^{n}(x_i^{\mathrm{obs}}-\bar{x}^{\mathrm{obs}})(x_i^{\mathrm{mod}}-\bar{x}^{\mathrm{mod}})/(n\sigma_{\mathrm{mod}}\sigma_{\mathrm{obs}})$, bias=$\frac{1}{n}\sum_{i=1}^{n}(x_i^{\mathrm{mod}}-x_i^{\mathrm{obs}})$ (in units of mg Chl m^{-3}) and ratio of standard deviations=$\sigma_{\mathrm{mod}}/\sigma_{\mathrm{obs}}$, where $\sigma_x=\sqrt{\frac{1}{n}\sum_{i=1}^{n}(x_i-\bar{x})^2}$ and the overbar denotes the mean.

Month	RMS	corr	bias	ratio of stdev
Apr	4.02	0.57	−1.29	0.62
May	5.23	0.64	1.55	1.19
Jun	6.85	0.64	1.24	1.36
Jul	6.53	0.68	1.69	1.08
Aug	5.89	0.61	1.14	1.00
Sep	3.74	0.59	−0.6	0.99

BGD
8, 121–156, 2011

Table 2. Linear correlation coefficients and p-levels for the delta region.

Variables	Correlation	p-level	significant at $p<0.05$?
PP and DIN (Oct–Feb)	−0.60	<0.0001	yes (highly)
PP and DIN (Oct–Mar)	−0.32	0.028	yes
PP and DIN (Oct–Apr)	0.32	0.016	yes
PP and DIN (Jun–Sep)	0.83	$<10^{-8}$	yes (highly)
PP and DIN (May–Sep)	0.63	<0.0001	yes (highly)
climatologies of PP and DIN (Jun–Sep)	0.99	0.01	yes
climatologies of PP and DIN (Jun–Oct)	0.99	0.001	yes
anomalies of PP over DIN (Jun–Sep)	0.81	$<10^{-7}$	yes (highly)
anomalies of growth rate and DIN (Jun–Sep)	−0.07	0.69	no
anomalies of Chl and DIN (Jun–Sep)	0.90	$<10^{-10}$	yes (highly)
PP and N load (Oct–Feb)	−0.56	<0.0001	yes (highly)
PP and N load (Oct–Mar)	−0.24	0.10	no
PP and N load (Oct–Apr)	0.30	0.026	yes
PP and N load (Jun–Sep)	0.86	$<10^{-9}$	yes (highly)
PP and N load (May–Sep)	0.70	$<10^{-6}$	yes (highly)
climatologies of PP and N load (Jun–Sep)	1.00	<0.0001	yes (highly)
climatologies of PP and N load (Jun–Oct)	1.00	<0.0001	yes (highly)
anomalies of PP over N load (Jun–Sep)	0.75	$<10^{-6}$	yes (highly)
anomalies of growth rate and N load (Jun–Sep)	−0.25	0.18	no
anomalies of phy and N load (Jun–Sep)	0.91	$<10^{-11}$	yes (highly)

BGD
8, 121–156, 2011

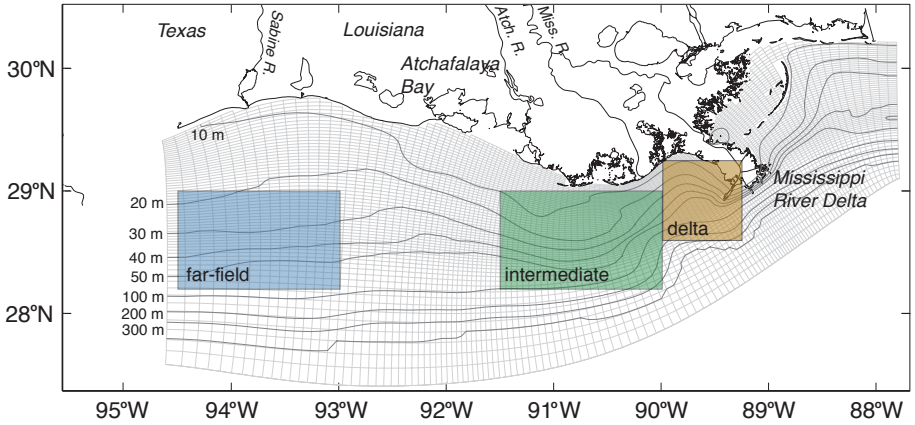

Fig. 1. Model domain and bathymetry. The colored boxes indicate areas used for averaging purposes and are referred to as delta (brown), intermediate (green) and far-field (blue) region in the text.

BGD
8, 121–156, 2011

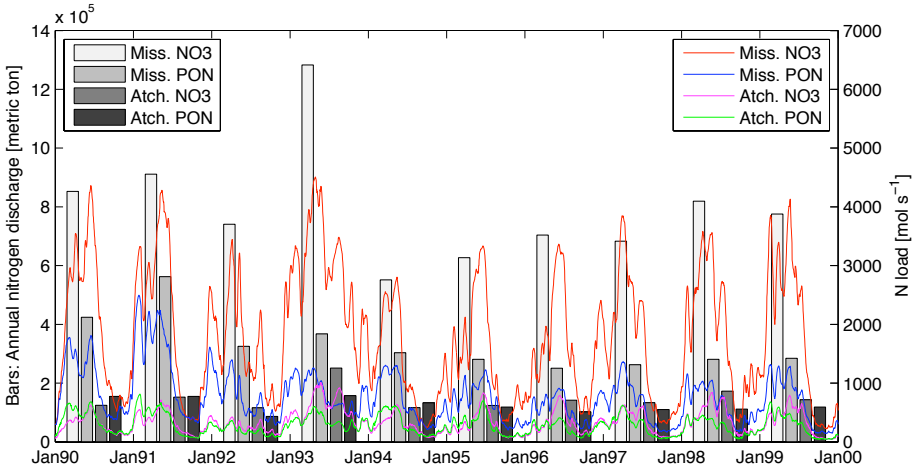

Fig. 2. Annual loads of nitrate and PON from the Mississippi and Atchafalaya Rivers (gray bars corresponding to *y*-axis on the left) and continuous loads used as model inputs (colored lines corresponding to *y*-axis on the right).

BGD
8, 121–156, 2011

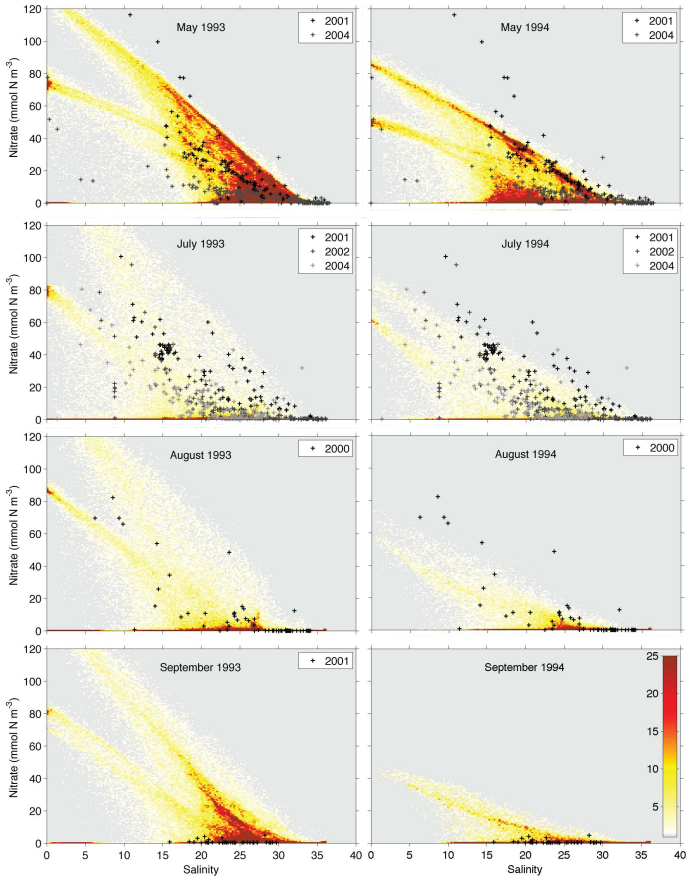

Fig. 3. Simulated surface nitrate concentrations are shown over salinity in form of a 2-dimensional histogram. All surface cell in the model domain are included. Color indicates the number of simulated nitrate-salinity-pairs per bin (see color scale in bottom right panel). Symbols represent surface nitrate measurements for the same months but different years (see legends).

BGD
8, 121–156, 2011

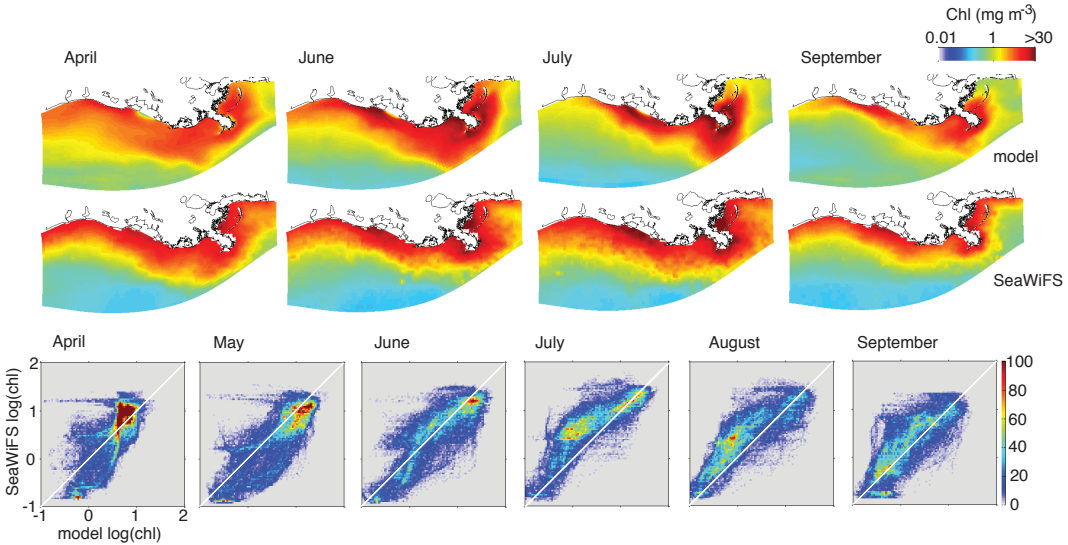

Fig. 4. Monthly climatology of simulated surface chlorophyll (top row) and surface chlorophyll from the SeaWiFS satellite (row below) for April, June, July and September. 2-dimensional histograms of SeaWiFS over model chlorophyll from April through September are shown in the bottom row. The 1-to-1 line is shown in white.

BGD
8, 121–156, 2011

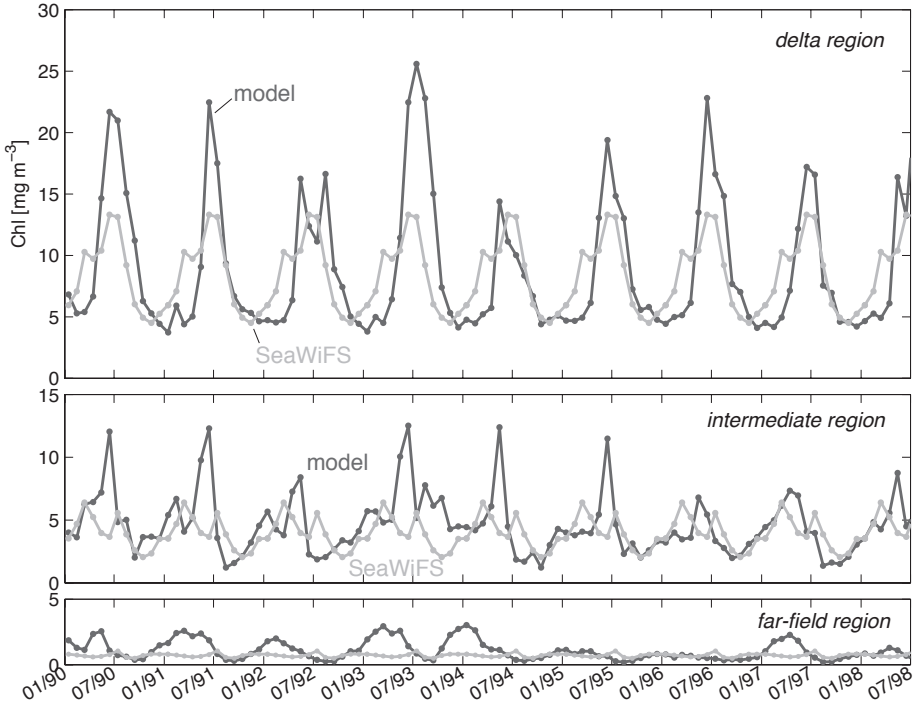

Fig. 5. Monthly mean surface chlorophyll concentrations in comparison to the monthly SeaWiFS climatology both averaged over the delta, intermediate and far-field regions.

BGD
8, 121–156, 2011

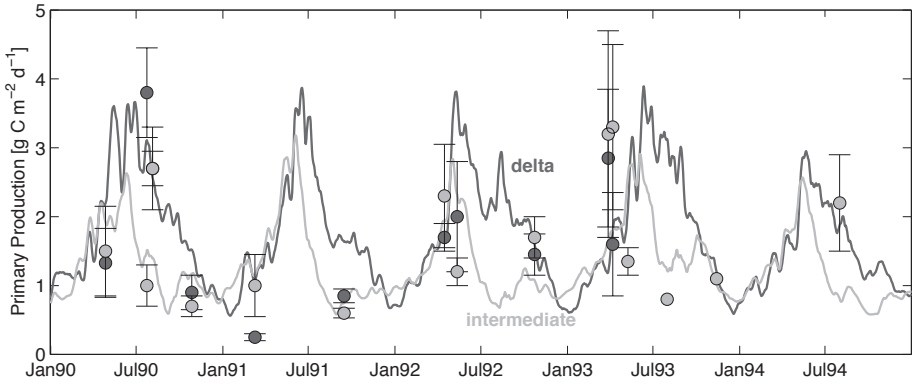

Fig. 6. Simulated primary production averaged for the delta and intermediate regions (solid lines) compared to measurements by Lohrenz et al. (1997) for the same regions (filled circles with errorbars represent mean and standard deviation). The dark and lights gray symbols and lines correspond to the delta and intermediate regions, respectively.

BGD
8, 121–156, 2011

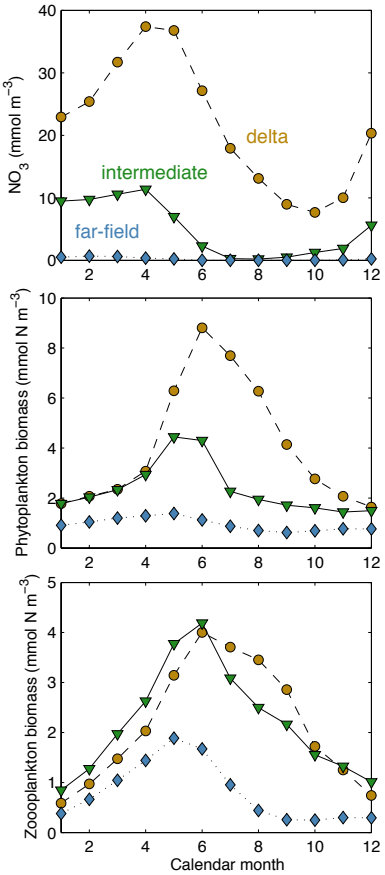

Fig. 7. Climatological monthly means of simulated mixed layer nitrate (top), phytoplankton (middle) and zooplankton (bottom) biomasses for the delta, intermediate and far-field regions (see Fig. 1). The mixed layer is here defined as the shallowest water depth at which temperature is at least 0.5 ˚C below the surface temperature.

BGD
8, 121–156, 2011

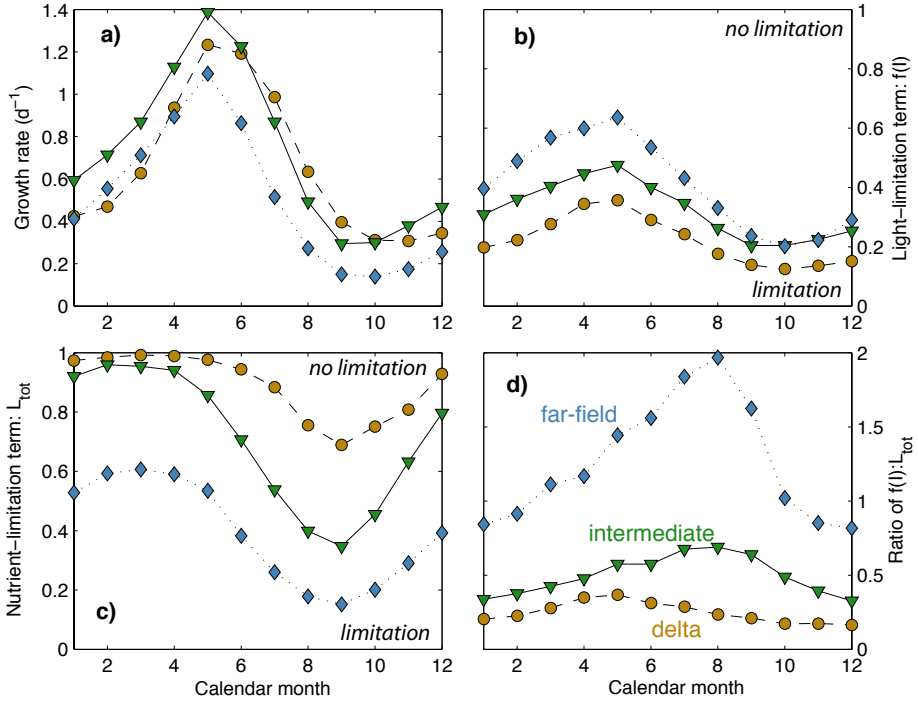

Fig. 8. Monthly climatology of simulated mixed layer mean phytoplankton growth rate **(a)**, light-limitation term **(b)**, nutrient-limitation term **(c)** and ratio of light- and nutrient-limitation **(d)** for the delta, intermediate and far-field regions.

BGD
8, 121–156, 2011

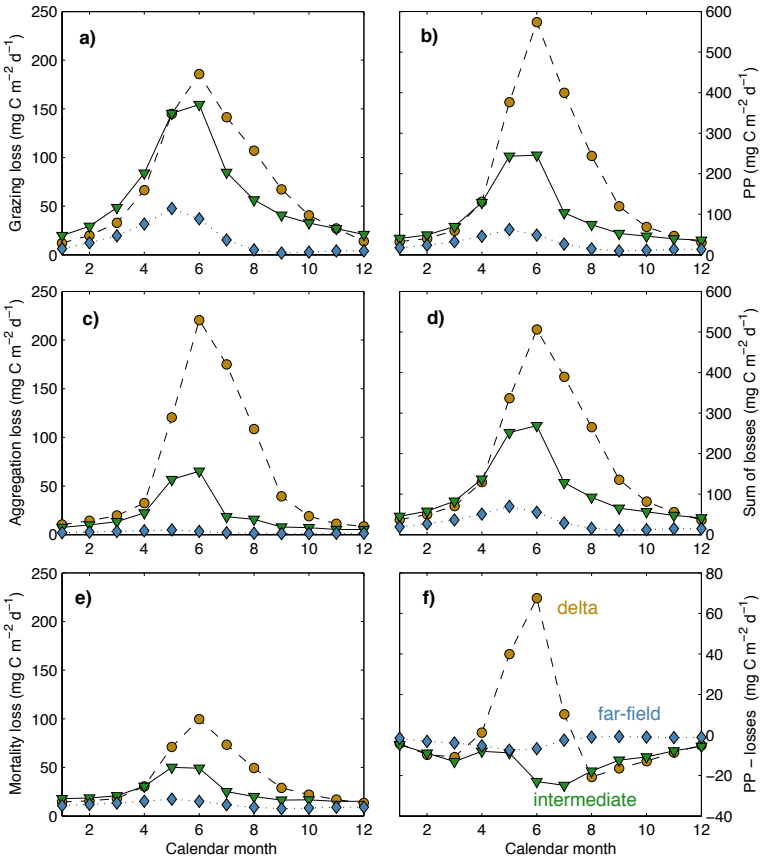

Fig. 9. Monthly climatology of simulated mixed layer mean phytoplankton loss due to grazing **(a)**, aggregation **(c)**, and mortality **(e)**. Also shown is monthly mixed layer mean primary production **(b)**, sum of the three biological phytoplankton loss terms **(d)** and balance of primary production and biological loss terms **(f)**.

BGD
8, 121–156, 2011

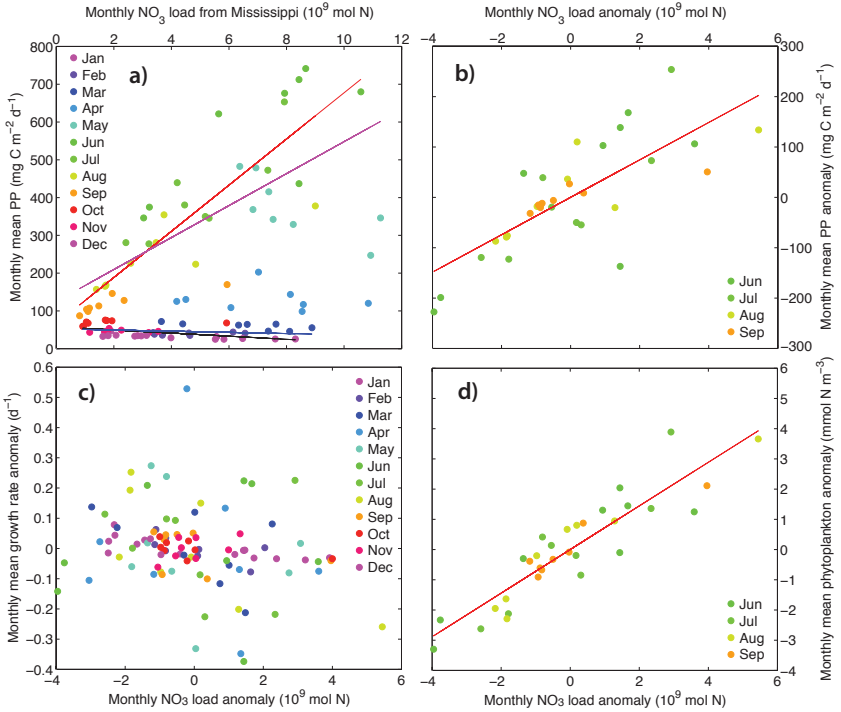

Fig. 10. Simulated monthly mean variables for the delta region plotted over monthly NO_3 load from the Mississippi River for the simulation period from January 1990 to December 1998. **(a)** Primary production over NO_3 load (colored dots) and their linear regressions (solid lines) for June through September (red), May through September (magenta), October through February (black), and October through March (blue). **(b)** Anomaly of primary production over anomaly of NO_3 load for June through September (colored dots) and their linear regression (red line). **(c)** Anomaly of phytoplankton growth rate over anomaly NO_3 load. **(d)** Anomaly of phytoplankton biomass over anomaly of NO_3 load (colored dots) and their linear regression (red line). Regression parameters are given in Table 2.

BGD
8, 121–156, 2011